

Precision manufacturing of a lightweight mirror body made by selective laser melting

Enrico Hilpert,^{1,2,*} Johannes Hartung,¹ Stefan Risse,¹ Ramona Eberhardt,¹ and Andreas Tünnermann^{1,2}

¹*Fraunhofer Institute for Applied Optics and Precision Engineering IOF, Albert-Einstein-Straße 7, 07745 Jena, Germany*

²*Institute for Applied Physics, Max-Wien-Platz 1, 07743 Jena, Germany*

(Dated: June 6, 2018)

This article presents a new and individual way to generate opto-mechanical components by Additive Manufacturing, embedded in an established process chain for the fabrication of metal optics. The freedom of design offered by additive techniques gives the opportunity to produce more lightweight parts with improved mechanical stability. The latter is demonstrated by simulations of several models of metal mirrors with a constant outer shape but varying mass reduction factors. The optimized lightweight mirror exhibits 63.5 % of mass reduction and a higher stiffness compared to conventional designs, but it is not manufacturable by cutting techniques. Utilizing Selective Laser Melting instead, a demonstrator of the mentioned topological non-trivial design is manufactured out of AlSi12 alloy powder. It is further shown that – like in case of a traditional manufactured mirror substrate – optical quality can be achieved by diamond turning, electroless nickel plating, and polishing techniques, which finally results in < 150 nm peak-to-valley shape deviation and a roughness of < 1 nm rms in a measurement area of $140 \times 110 \mu\text{m}^2$. Negative implications from the additive manufacturing are shown to be negligible. Further it is shown that surface form is maintained over a two year storage period under ambient conditions.

Selective Laser Melting Lightweight Design Diamond Turning Metal Mirror AlSi12 Additive Manufacturing

I. INTRODUCTION

Additive Manufacturing (AM) is regarded as the next industrial revolution. While applications in the medical field exist for some time now, AM has constantly evolved and is being used in the automotive, civil aviation, military and aerospace sector today. Due to widespread research the pool of available materials is constantly growing. Titanium and aluminum alloys are widely used material systems for structural and lightweight applications due to their low density and high stiffness. While the machinability of titanium is difficult, aluminum is easy to process [1, 2]. Low density and cost-effective manufacturing render it also a good choice to produce high performance optical elements. Traditionally, aluminum mirrors are produced using several manufacturing and finishing steps resulting in very good shape accuracy (dependent on mirror size) and roughness values of < 0.5 nm rms [3]. Various aluminum alloys are used for production of the mirror substrates, Al 6061 being the dominant material due to its high temporal stability [2]. Targeting applications in the infrared spectral range, precise diamond turned Al 6061 is sufficient as the turning pattern does not interfere with the respective wavelengths [2, 4]. For visible and shorter wavelengths, a polishable layer is necessary to generate smoother surfaces and remove the turning marks that cause deteriorating scattering of the desired radiation. X-ray amorphous electroless nickel is a state of the art functional layer for high performance polishing [5]. Though, electroless nickel and aluminum alloys differ regarding their coefficients of thermal expansion. Due to this mismatch shape changes of the part occur when thermal loads are applied (bimetallic bending). By using aluminum with 40 wt% silicon (AlSi40), this thermal mismatch is reduced to a minimum [6]. Beside the optical and mechanical performance of metal mirrors, their weight is an important factor when highly dynamic scanning applications are desired or when mirrors are used in optical systems in space. The reduction of weight by cutting techniques is a common method but its extent is limited due to the accessibility of the interior material by manufacturing tools. Mirrors consisting of several joined parts or with open backsides are two approaches to increase the mass reduction at the expense of stiffness. Yet, monolithic mirrors are ideally suited for space applications due to the absence of adhesives. Also, a closed backside is desirable as the mechanical stability compared to open backside mirrors is higher [7]. Additive Manufacturing is a promising solution to optimize both mass and mechanical stability to a higher level than approachable by conventional techniques. Selective Laser Melting (SLM) is a specific AM technique, which generates parts out of powder on a layer by layer principle. This enables the manufacturing of complex internal structures and thus, offers a high mass saving potential. The front and back faces of such metal mirrors can

* enrico.hilpert@iof.fraunhofer.de

remain completely closed, because there are no cutting tools necessary to generate the lightweight structure. In this work, SLM is used to manufacture a hollow structured monolithic metal mirror, thereby substituting conventional machining processes. This is realized by employing aluminum with 12 wt% silicon (AlSi12) because alongside the also near eutectic AlSi10Mg alloy it is the most well-understood aluminum material for powder bed based Additive Manufacturing processes [8–12]. Besides the generation of the mirror body by the new technique mentioned a well-established manufacturing chain for producing a high quality metal mirror is applied. It should be demonstrated that metal mirrors with optical properties at an ultra-precise level are manufacturable by additive processes, also showing the reduction of mirror mass to values that are not achievable by conventional fabrication techniques.

The article is divided as follows. In sect. II, a short outline over the state of the art of AM for optical applications is given. Section III contains the Computer Aided Design (CAD) model descriptions, mandatory definitions necessary for the investigation, and the evaluation of different mirror design variants per Finite Element Analysis (FEA). In sect. IV, the manufacturing via SLM together with a quality inspection and the post-finishing are discussed for one single design, also considering the temporal stability. Section V contains conclusions and an outlook for future investigations in the context of AM for metal mirrors.

All computations are conducted using the finite element program ANSYS [13]. Further, roughness measurements of machined surfaces are carried out by a Zygo New View 600 White Light Interferometer, while roughness of the SLM part as-built is determined by a Taylor Hobson Talysurf profilometer. The shape of the optical surface is measured using a Zygo GPI XP/D 1000 interferometer. Interior building quality is analyzed by 3D X-ray tomography utilizing a Phoenix v|tome|x L 240.

II. STATE OF THE ART

Additively manufactured metal mirrors have hardly been researched so far. One study shows a mirror made of Al 6061, which was replaced by an additive design made out of Ti6Al4V achieving a mass reduction of 54 % using lattice structures [14]. In [15] several approaches are discussed to manufacture mirrors by additive techniques considering various designs and materials.

Also, the feasibility to use AlSi10Mg and Ti6Al4V to produce mirrors by additive techniques, including grinding and polishing post-processes, was investigated in [16, 17]. The main challenges reported by the authors are porosity of the additive manufactured material as well as the complexity of the CAD models which were developed for the AM process. Due to the huge amounts of elements, modal and thermal simulations become complicated to run and require a lot of time. In spite of that, the potential of tailored designs made by additive manufacturing is regarded very high. Topology optimized and bionic structures for metal mirrors are also of particular interest as they offer a good compromise between mechanical functionality and material usage. These are under current investigation by the authors of [16, 17].

In contrast to the design of metal mirrors studies regarding the optimization of brackets, support structures, and housings for space applications are available in the literature [18–20].

III. MIRROR DESIGN, SIMULATION AND DESIGN EVALUATION

A. Design study

As an initial study, five different mirror designs are investigated. Primarily, the mirror body is based on a cylindrical geometry, measuring 86 mm in diameter. The optical surface exhibits a spherical concave shape, with a radius of curvature of 200 mm, while the backside is flat. Optical front and backside as well as the circumferential face of the mirror are completely closed. The described design represents a full solid mirror without mass reduction. Additionally, four mass-reduced designs with the same outer dimensions are considered for a later comparison. The first one is an empty shell model, which represents the theoretical limit of mass reduction for the present investigation in case of a closed mirror. Here, the term “empty” refers to the complete removal of the interior, while the remaining shell exhibits wall thicknesses of 2 mm at front and back and 1 mm at the circumference. Fig. 1 shows the second model, which contains holes in a cross directional pattern along the neutral plane and represents a lightweight design manufacturable by cutting techniques [4, 5].

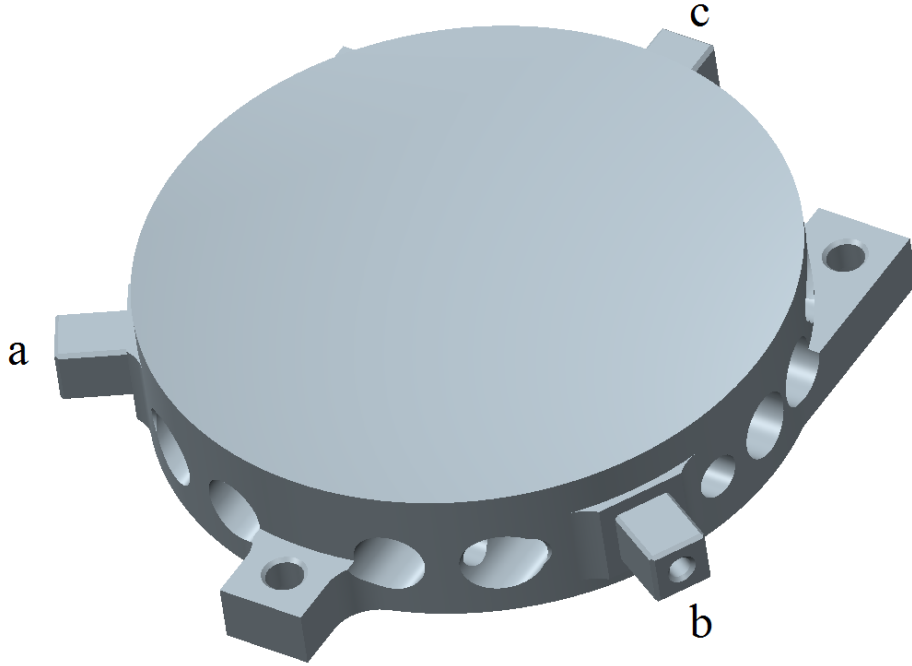


FIG. 1: CAD model of the “drill” mirror

Third, a novel lightweight design, the “honeycomb” mirror, was developed, which is only manufacturable by Additive Manufacturing. The inner part of the mirror consists of a hexagon (honeycomb) structure, with additional holes on all faces. Further, this design features multiple holes with a diameter of 4 mm each on the circumferential face, which allows a complete removal of any unmolten powder, which remains inside of the hollow structured mirror body during SLM. Front and backside of the design, as in the first two models, are completely closed. All relevant wall thicknesses for the honeycomb design are given in table I. The front and back faces are chosen to be thicker than the circumferential face to ensure a minimum remaining thickness after manufacturing steps. The thickness of the interior walls is designed to be as thin as possible, regarding the SLM machine limits.

TABLE I: Measures of the honeycomb mirror in mm, t gives wall thickness, $d_{\text{honeycomb}}$ represents diameter of inscribed circle of hexagon cells

t_{front}	t_{back}	$t_{\text{circumference}}$	$t_{\text{honeycomb}}$	$d_{\text{honeycomb}}$
2.0	2.0	1.0	0.6	9.3

The last design is an identical “honeycomb” mirror, in this case with the back side removed, which yields open hexagon cells. This is a common technique for the production of lightweight mirrors and should therefore serve as a state of the art design [7]. This model does not exhibit the inner and circumferential holes of the previous one as it is manufacturable by conventional cutting techniques. Fig. 3 shows the CAD design from the back.

For evaluating the degree of mass reduction of different designs, the mass reduction factor L is used, which relates the mass m of the corresponding design variant to the mass of the solid model m_{Solid} , via

$$L = 1 - \frac{m}{m_{\text{Solid}}}, \quad (3.1)$$

where L is calculated in %, see table II.

TABLE II: Mass reduction factors [%] of the mirror designs used in the FEA

Solid	Drill	Honey	HoneyNB	Empty
0.0	25.5	63.5	70.4	68.2

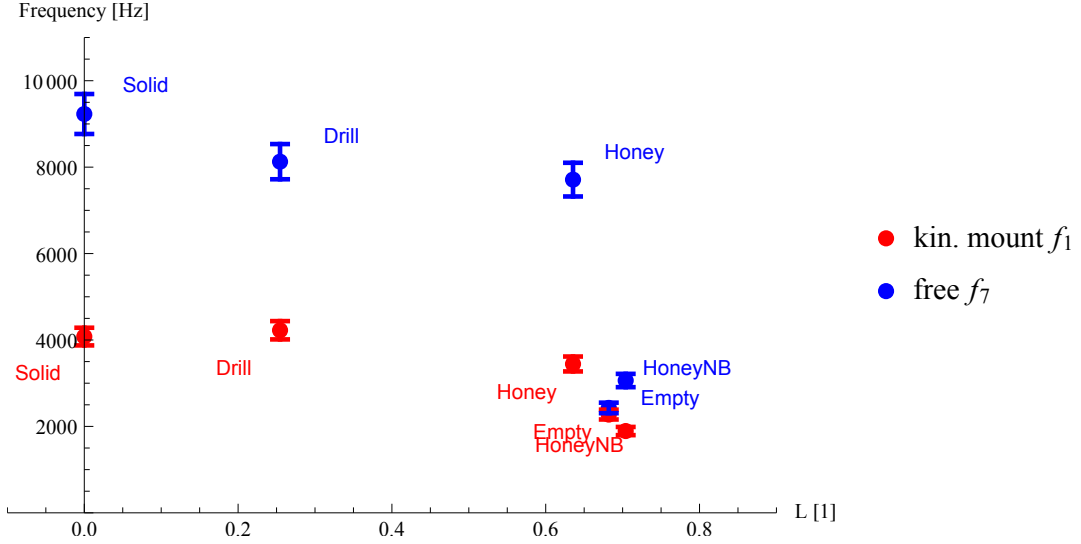


FIG. 4: Mass reduction factor versus modal frequency of CAD designs. Errorbars indicate deviations from the center eigenfrequency due to variations in Young’s modulus E of $\pm 10\%$ which corresponds to ± 7.5 GPa.

The “honeycomb” mirror (see fig. 2) has a mass of about $m_{\text{Honey}} \approx 104$ g, which corresponds to $L \approx 63.5\%$ compared to the solid body ($m_{\text{Solid}} \approx 286$ g). All models have three mounting brackets, marked with a–c in fig. 1. These are used as clampings for FEA and as references for quality inspection, see sect. IV.

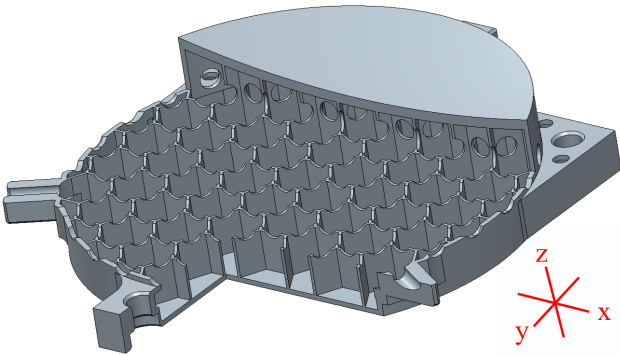


FIG. 2: CAD model of the honeycomb mirror with sectioning planes added to demonstrate the hollow structure

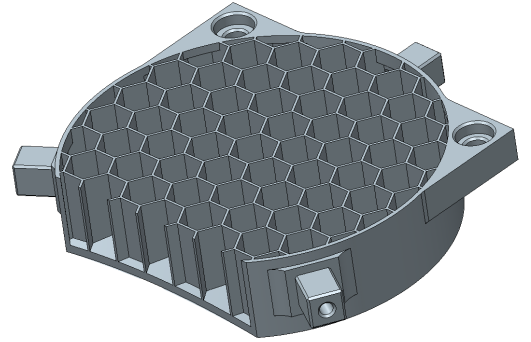


FIG. 3: Honeycomb mirror with open backside, upside down

B. Simulation

To evaluate the stiffness of the mirror designs, a modal analysis is performed using a slightly simplified model with some curvatures, chamfers, and holes removed. The mirrors are analyzed in two different mounting setups. These are given by a kinematical mounting and a setup without any mounting (denoted as “free”). The kinematical mounting fixes exactly six degrees of freedom (DOF) of the part, which means that two tangential DOF are fixed and the radial DOF is unconstrained at the mounting structures a, b, and c in fig. 1. “Free” mounting means that translational and rotational motions may appear under certain load cases. In a modal analysis, this leads to six zero-modes (one for every DOF). The resulting eigenfrequencies in connection with the mass reduction factor L in (3.1) are a measure for the stiffness of the designs. Fig. 4 shows the first eigenfrequency f_1 and f_7 , respectively, over L for the three mirror models in the different mounting setups. The first six zero-modes of the “free” setup are omitted (therefore f_7). It is shown that the “honeycomb” mirror exhibits a nearly equal stiffness (eigenfrequency), despite being more lightweight than the “drill” model. The empty shell model and open back structure are distinctly less stable.

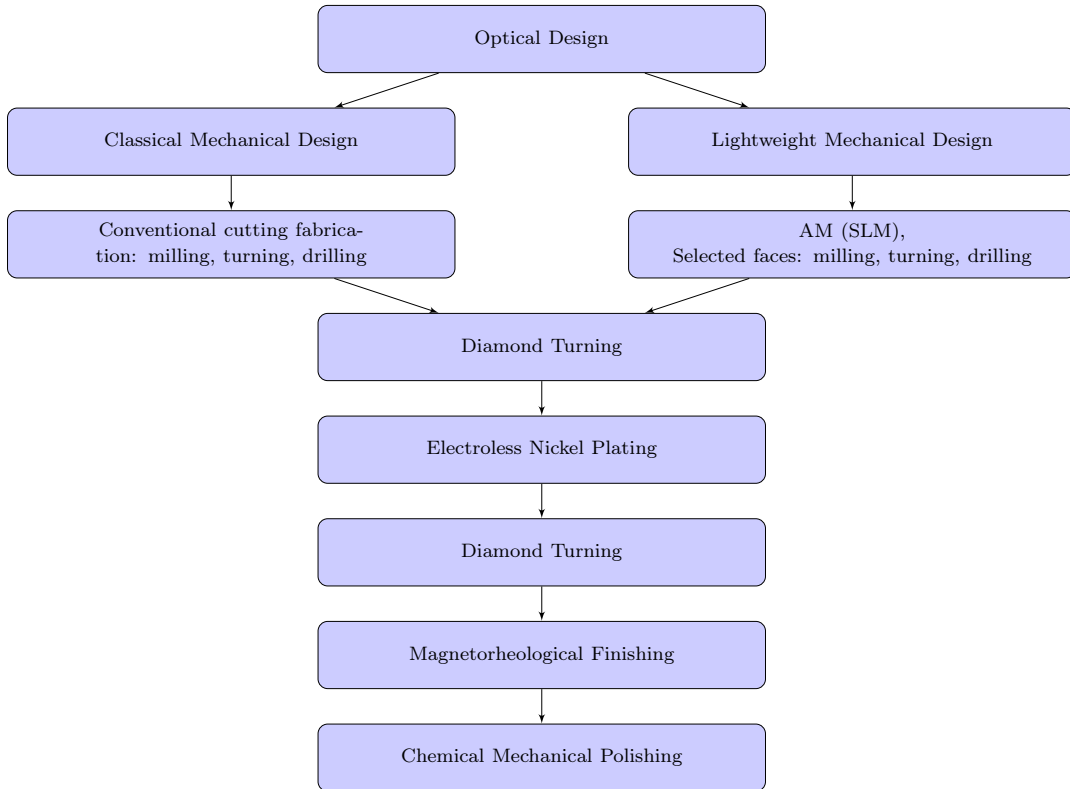


FIG. 5: Process chain to generate mass reduced metal mirrors. After the additive manufacturing, usually another step is necessary to produce appropriate mounting planes or other non-optical functional surfaces. Lightweight design in this context means: the mechanical design cycle for some topological non-trivial interior structures including an FEA step for optimization.

IV. MANUFACTURING AND POST-FINISHING

A. Process chain

After showing the superiority of the “honeycomb” design, the manufacturing of the mirror body is being demonstrated. Fig. 5 shows the process chain for the production of metal mirrors which will be applied. The conventional machining processes are complemented by SLM, while the following steps remain feasible on the novel manufactured mirror body. After additive manufacturing by SLM and stress relieving, the optical surface of the mirror will be diamond turned, electroless nickel plated, and finished including the final polishing step.

B. Additive Manufacturing of the mirror body

In preparation of the manufacturing, the CAD model of the mirror body is virtually aligned in the building chamber as shown in fig. 6. In order to stabilize the part, support structures are used on the outer faces. These are thin lattices of material, which are selective laser melted along with the mirror during the process and mechanically removed after finalization. The tilt angle of 41° is chosen to minimize overhang features and critical angles, which are difficult to generate without support structures (supports have to be avoided in the mirror interior) [21, 22]. The term “overhang” refers to all faces whose surface normals are pointing towards the building platform (orange box in fig. 6). A Concept Laser M2 Cusing SLM machine is used to build the mirror substrate. AlSi12 alloy powder with a particle size of $<25\ \mu\text{m}$ and spherical shaped particles is applied for manufacturing, utilizing nitrogen as shielding gas. The layer thickness measures $25\ \mu\text{m}$ for the actual part and $50\ \mu\text{m}$ for the support structures, which means supports are generated every second layer. The illumination of the part is done in a continuous pattern, which means single lines are scanned next to each other in the volume, finalized by a contour line on the outer and inner surfaces. Details about

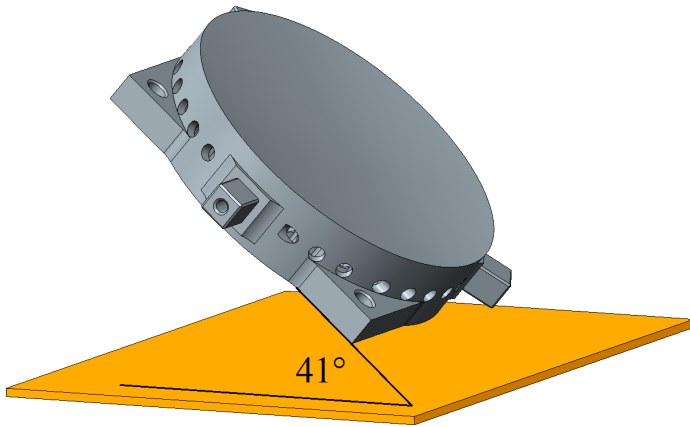


FIG. 6: CAD model of honeycomb mirror in building orientation

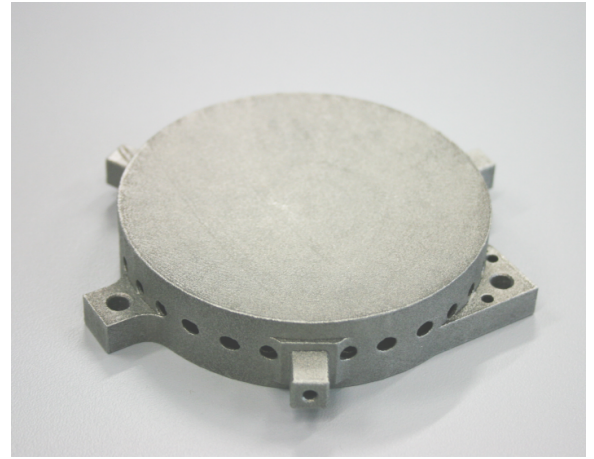


FIG. 7: Mirror body after SLM and cleaning

the laser parameters (scanning velocity, average power, hatching distance) are not available as they are protected by the machine vendor.

After SLM the powder is removed from the interior of the mirror using the holes on the circumferential and interior faces. First, this is carried out while still working in the glovebox of the SLM machine under inert atmosphere. Next step is the separation of the mirror from the building platform and support structures using a saw. Due to the utilization of tapered geometry at the joint to the mirror, the remaining support structures could be easily separated manually. Eventually, cleaning procedures could be carried out, which included several wet rinsing and ultrasonic steps. Fig. 7 shows the mirror substrate at this point. Considering the cleaning it shall be noted that the size of the holes should be increased in order to promote better fluid flow and reduce cleaning time.

C. Quality inspection

The outer surface of the mirror body shows a typical roughness for SLM processed parts ($>5 \mu\text{m } R_a$) and strongly depends on the orientation of structures with respect to the powder layers or building direction. In general, all faces that are oriented towards the building platform show increased roughness, which can be mainly attributed to powder particles adhering to the melt pool from the bottom. Similar results were found by other researchers, too [21]. The outer holes on the circumferential face show elliptical shape with blunt edges, which is a result of overhanging geometry. The measures show variations of up to $200 \mu\text{m}$ in positive direction mostly (excess material). As a consequence outer bores are too small and show high roughness on overhanging areas. This, under some circumstances, makes post manufacturing necessary, which arises the question whether outer bores should be generated by SLM at all. This should be decided depending on the tolerances needed.

Internal geometry is examined using 3D computed tomography [23]. This generates a three dimensional voxel model, which is then compared to the CAD model. The size of the scanned part allows a scanning resolution of $60 \mu\text{m}$. The scan is performed in the xy and the yz plane, with reference to the coordinate system in fig. 2. The data shows that the inner hollow structure is generated completely. Coarse errors such as porosity, missing or unintended structures are analyzed by evaluating the two-dimensional cross sectional images. Only one pore (see fig. 8, white circle) is detected in the images, which shows a good building quality. Its size of 1.5 mm is determined by analyzing the X-ray pictures using the voxel size.

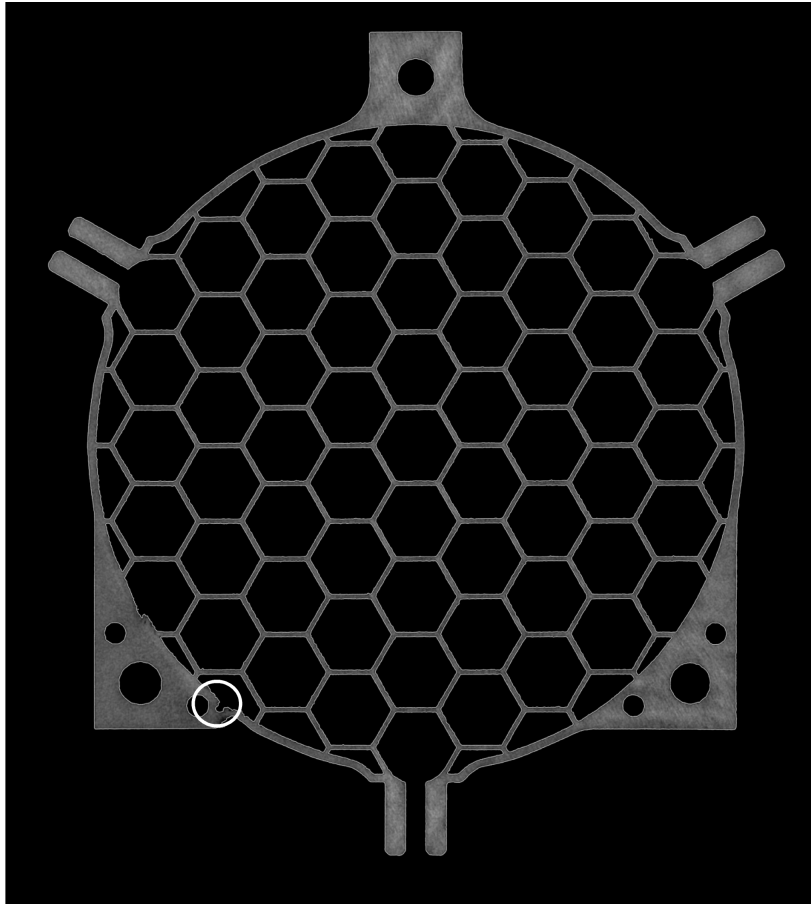


FIG. 8: Building error revealed by X-Ray tomography

Due to the extent of the pore, its origin is most likely caused by an erroneous layer generation during SLM, for example because of missing powder at this specific location. The powder coating is done by a rubber blade, which is prone to warping of already solidified material. If the part warps (because of residual stress) the rubber bends around it and quickly moves onward once the warped area is passed. This leads to zones of missing powder directly behind this geometry. Also, material evaporation by the laser radiation can be excluded as an origin of the pore because this type of pores cannot be larger than the melt pool. An online monitoring of the SLM process (e.g. camera images of each layer) could provide more details about such defects, but was not used during the building. Other inhomogeneities such as small grooves or increased roughness (adherence of particles) are occasionally found in the X-ray images.

D. Finishing operations

Subsequent to the SLM process, the cleaned mirror substrate is artificially aged using an appropriate heat treatment. This is necessary to reduce stress induced during the laser melting process, which is caused by very high thermal gradients. These effects are an inherent problem of many additive manufacturing processes and therefore subject to intensive research [11, 24–27]. After heat treatment the front and back sides of the mirror have to be milled. The part, showing near net shape already, is therefore aligned using the circumferential face for centering and the mounting structures (a–c, see fig. 1) to get the z position. In this step support structures from the back face are removed and the front surface is smoothed for diamond turning. The closed backside of the mirror substrate renders advantageous for this technique, because a vacuum chuck is applicable for mounting on the turning machine. For proper function, planarity of the backside is established using a lapping process after the milling. By utilizing this procedure, a mechanical mounting or application of adhesives is avoided. The following ultra-precise diamond turning is carried out in two passes. This reduces the roughness of the optical surface and establishes the target shape, which allows the measurement of both parameters by optical techniques. The resulting surface roughness is measured using

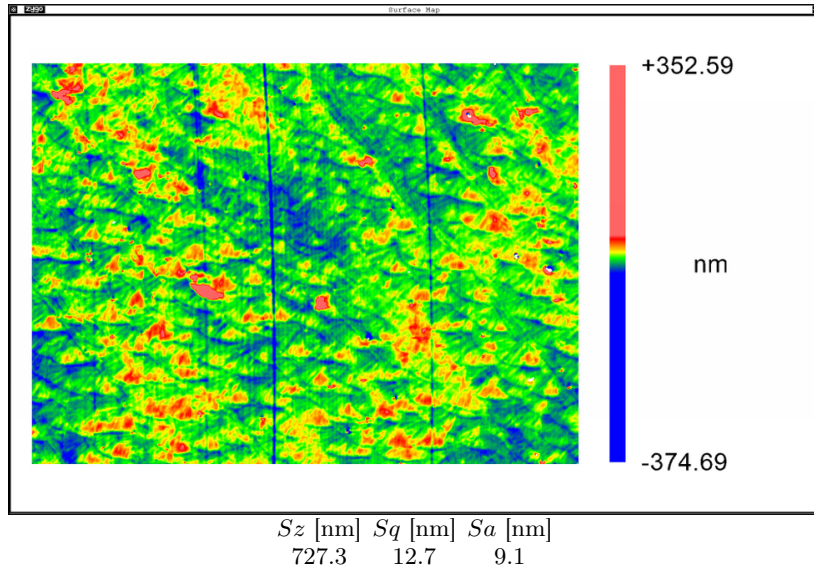


FIG. 9: Surface roughness @ $2.8 \times 2.1 \text{ mm}^2$ after diamond turning of AlSi12 body; feed direction: horizontal, tangential direction: vertical

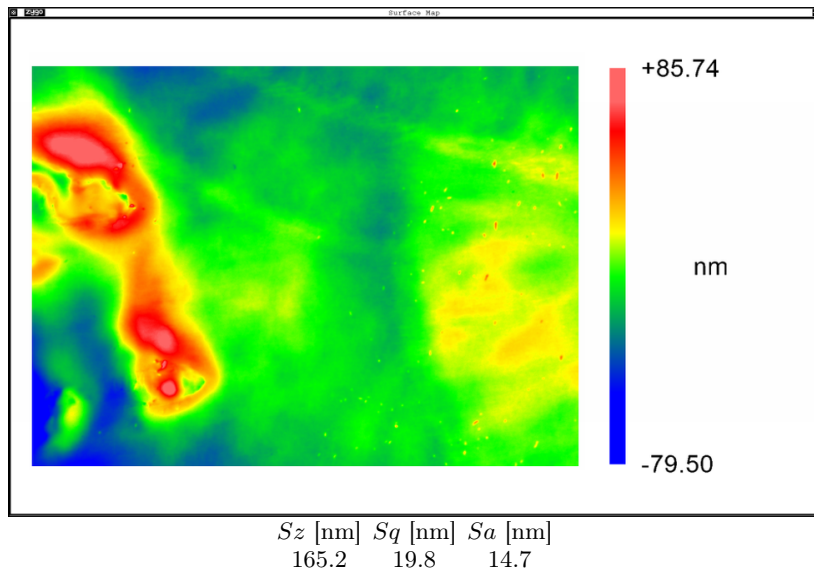


FIG. 10: Surface roughness @ $140 \times 110 \mu\text{m}^2$ after diamond turning of AlSi12 body

a white light interferometer with a $2.5\times$ lens covering an area of $2.8 \times 2.1 \text{ mm}^2$, see fig. 9. Turning marks are hardly visible (feed direction is horizontal, tangential direction is vertical in the image), which can be attributed to brittle silicon particles leading to high cutting forces and therefore rougher surfaces compared to Al 6061 [3, 7]. As a result, the value of Sz is very large compared to the averaged roughness values, which can be attributed to outliers due to the silicon particles.

Fig. 10 shows the roughness using a $50\times$ lens, covering an area of $140 \times 110 \mu\text{m}^2$. An elevated particle is visible, which mainly contributes to the roughness.

The polycrystalline and multi-phase AlSi12 material can not be manufactured to sufficient roughness values. Therefore, an electroless nickel layer is plated onto the complete mirror substrate to surmount these limitations. The process parameters during electroless nickel plating have been tailored to incorporate 11 to 12 wt% phosphorus into the layer. As a result, the material is X-ray amorphous [28]. This condition in combination with resulting hardness values of 500 to 600 HV 0.1 ensures good machinability of the mirror surface [29–31]. The plating duration was adjusted to achieve a thickness of $100 \mu\text{m}$, which provides a dense structure even after removal of several micrometers of material



FIG. 11: Mirror mounted on diamond turning machine

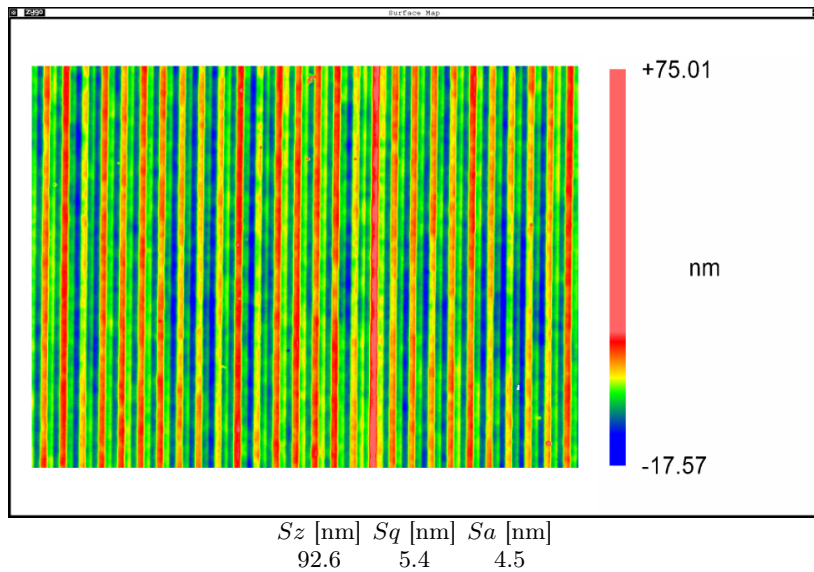


FIG. 12: Surface roughness @ $140 \times 110 \mu\text{m}^2$ after diamond turning of electroless nickel plated mirror substrate

by the following manufacturing steps [28, 32].

After the plating procedure, the mirror is heat treated and undergoes temperature cycling. A subsequent diamond turning procedure reestablishes the target shape and reduces roughness after plating. Fig. 11 shows the mirror mounted on the precision diamond turning machine at this step. The roughness after turning measures 5.4 nm Sq in the $140 \times 110 \mu\text{m}^2$ area, the turning marks are well defined, see fig. 12.

In a next step the optical surface is processed by Magnetorheological Finishing (MRF), which is capable of performing local shape corrections with high accuracy [33]. The mechanism of local shape correction on electroless nickel plated metal mirrors as well as further process details can be found in [34]. Fig. 13 shows the interferometric measure-

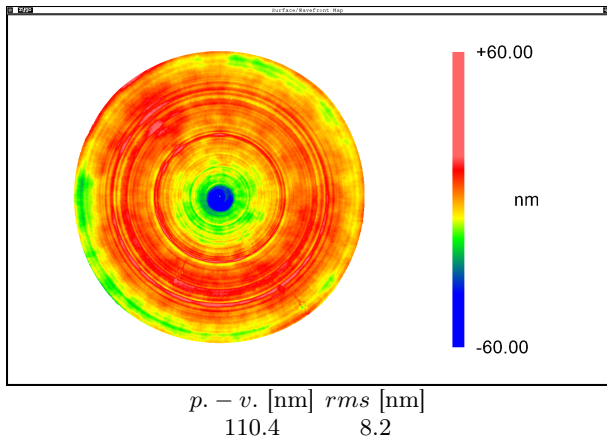


FIG. 13: Surface shape deviation after MRF

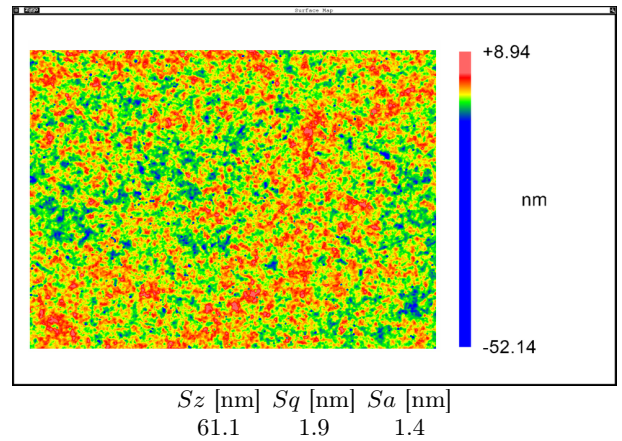
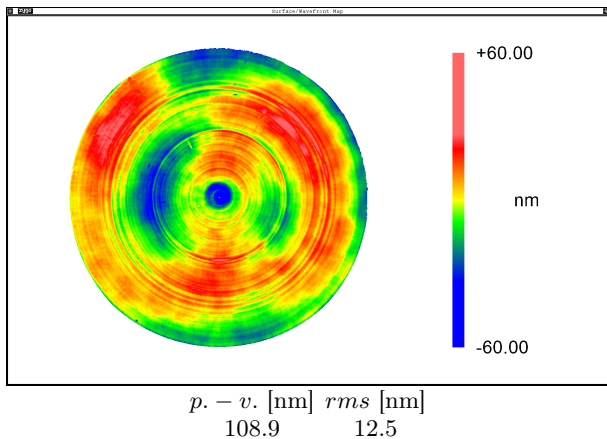
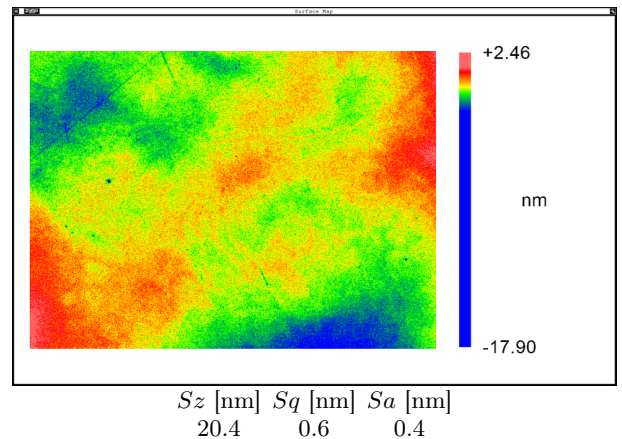
FIG. 14: Surface roughness @ $140 \times 110 \mu\text{m}^2$ after MRF

FIG. 15: Surface shape deviation after CMP

FIG. 16: Surface roughness @ $140 \times 110 \mu\text{m}^2$ after CMP

ment of the shape after this step. For analysis of the shape deviation, alignment contributions piston, tip/tilt, and power are subtracted from the resulting data. The remaining error of 110.4 nm peak-to-valley and 8.2 nm rms therefore represents the deviation from the best-fit spherical shape. In order to remove edge effects from manufacturing and measurements, the clear aperture was set to 81 mm for all shape analyses. The surface roughness @ $140 \times 110 \mu\text{m}^2$ is reduced to 1.9 nm Sq , showing an island-type morphology, which could be an indication of local variations in material removal rate, see fig. 14. After correction of the shape and improvement of roughness of the optical surface, Chemical Mechanical Polishing (CMP) is carried out to smoothen the optical surface, which further reduces the roughness. Fig. 15 shows the shape deviation after polishing, which is only slightly influenced compared to the state after MRF. The roughness is improved to values of <0.6 nm Sq , see fig. 16.

E. Final evaluation and temporal stability

In ground-based optical systems, particularly in space applications, the long-term stability is an important cost factor. Metal mirrors can be designed to sustain a long operating life. In order to achieve this, the mirror substrate material has to be optimized regarding its dimensional stability. Even small changes in the material, e.g., because of residual stress, may cause the whole element to fail its function over time [35]. In order to evaluate the additive manufactured mirror regarding temporal stability, the finished part was stored at ambient conditions for two years. In case of structural modifications like creep or relaxation effects, the shape would change and by that deteriorate the optical performance. Therefore, the interferometric shape measurement was repeated after two years using the same measurement setup. Fig. 17 shows the shape deviation after this time duration. The measured mean values did not

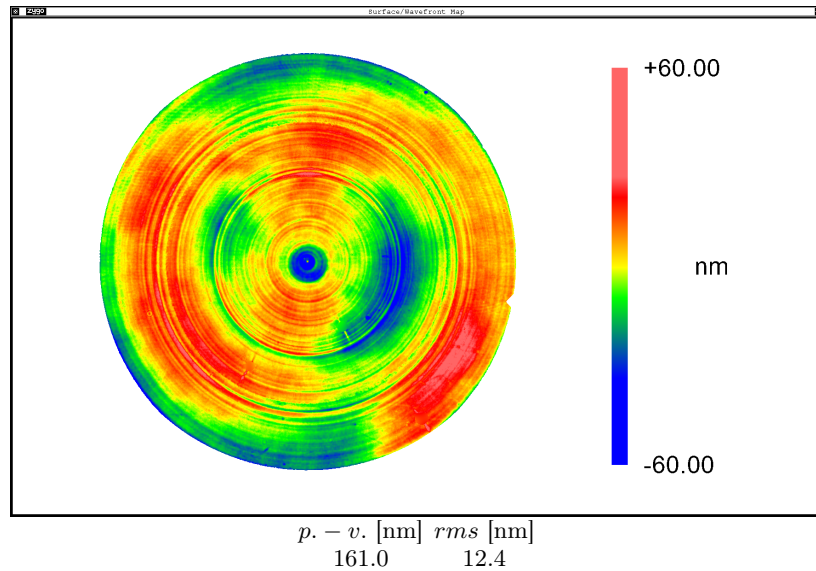


FIG. 17: Surface shape deviation after storage for two years at ambient conditions

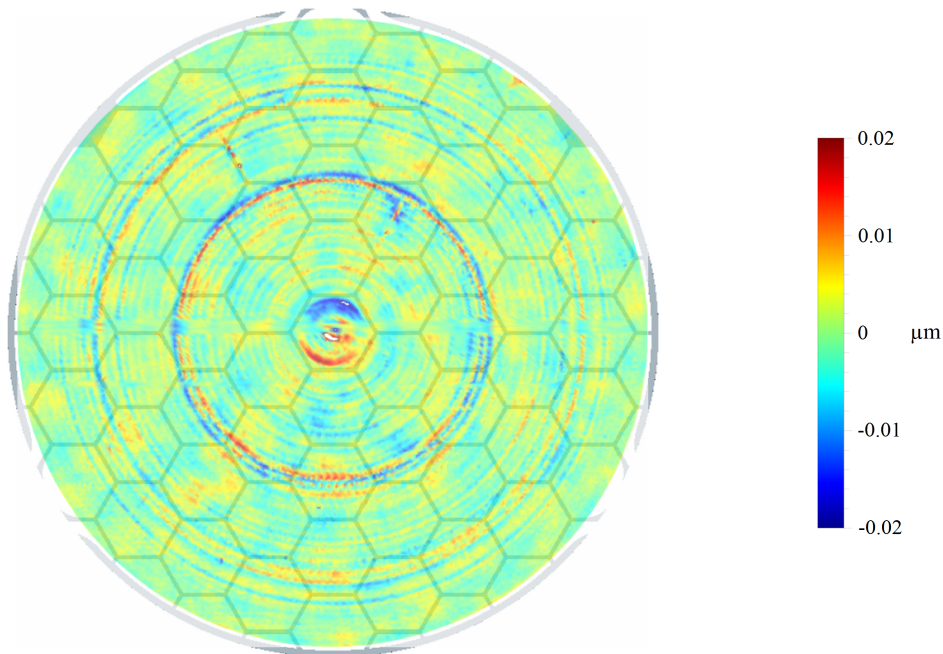


FIG. 18: Surface shape deviation with CAD interior overlay

change significantly (12.5 nm rms) in comparison with the results shown in fig. 15 (12.4 nm rms), also considering the measurement accuracy of ≈ 1 nm rms (notice that the p.-v. values are not a good indication of shape changes due to their sensitivity to outliers). By the process chain applied, the material has been brought into a condition, where plastic deformations do not occur at a temperature of 20 °C. Therefore, the mirror can be considered as dimensionally stable at the ambient conditions taken into account. In order to evaluate the influence of the mirror design on the shape accuracy regarding the applied manufacturing chain, surface shape deviation is analyzed in more detail. In contrast to classical mechanical designs the optical surface of the honeycomb mirror is thinner (2 mm thickness in CAD, >3 mm in classical designs) and could therefore be more prone to deformation under pressure (e.g. while polishing), where no interior walls are present, while at supported areas the surface remains unchanged. This would lead to an undesirable shape change, manifesting in a pattern as a representation of the interior structure.

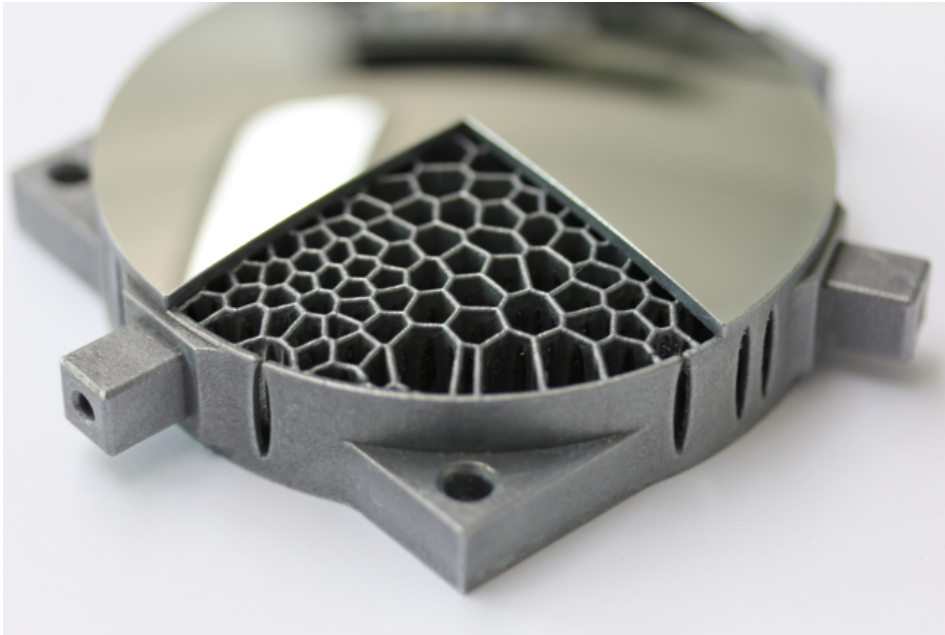


FIG. 19: Diamond turned mirror with non-trivial interior structure

The analysis was performed by using the interferometric measurement (see fig. 17) to get the deviation of the mirror surface from the optical design pattern. This deviation contains several spatial frequencies. The specific part of interest should have a frequency higher than the standard surface form error. Therefore, all Zernike polynomials up to very high orders were subtracted. This leads to visible small effects at the outer parts of the mirror and repeating pattern of peaks that are up to 7 nm high and separated by a distance of 10 mm which is almost equal to the hexagon diameter (see fig. ??). This result shows that the mirror surface is stiff enough to resist manufacturing loads by turning and polishing techniques, which is an indication that the design is well suited for the applied manufacturing chain. It is expected, however, that a smaller diameter of the hexagon cells is beneficial for stability.

V. CONCLUSIONS AND OUTLOOK

This study shows the suitability of Additive Manufacturing, i.e. Selective Laser Melting, for the production of parts for precision applications. Aiming at an improved mass reduction and high stiffness, a metal mirror design consisting of interior honeycombs is developed. By exploiting the freedom of design from additive processes, it is now possible to build such interior structures, while the backside remains closed, which is beneficial for stiffness and simplifies the manufacturing. Numerical simulations show that the honeycomb design outperforms conventional approaches.

The complex interior geometry makes a quality assurance necessary, which X-ray tomography is a suitable tool to work with. Missing or unintended structures can be visualized and processes can be adapted, respectively. Due to the limited shape accuracy of SLM fabrication, CAD models have to be tailored using offsets, where necessary. The present work shows a complete manufacturing chain, including additive manufacturing, diamond turning, magnetorheological finishing, and chemical mechanical polishing. The shape accuracy and roughness, which were achieved, make the mirror substrate suitable for optical applications up to the visible spectral range. As a result, it is shown that AlSi12 is a suitable aluminum alloy to generate metal mirrors, in addition to AlSi10Mg and Al6061 which have been demonstrated in the literature so far [16, 17]. These findings are supported by temporal stability measurements under steady ambient conditions which show no significant changes over a period of two years. Materials, which are thermally matched to electroless nickel (e.g. hypereutectic aluminum silicon alloys) are of particular interest because of a reduced bimetallic bending during varying temperatures [6]. Aluminum with a silicon content of 40 wt%, manufactured by SLM, is under present investigation. The application of additive manufactured mirrors in space environment requires further studies regarding the properties of the raw material.

Future work will also address the development of load case optimized non-trivial designs with a focus on even more lightweight mirrors. Fig. 19 shows an outlook on a possible advanced design. This demonstrator shows an ultra precise diamond turned optical surface and a part of the interior structure, which was manufactured using stochastic interior cells. All features, like elliptical holes and smaller wall thickness were chosen due to the results gathered

within the present study. The design development as well as other approaches will be the scope of a forthcoming publication.

ACKNOWLEDGEMENTS

The authors are grateful to the involved colleagues at Fraunhofer IOF, especially Robert Jende, Matthias Beier, Roland Ramm, Christoph Damm, and Nils Heidler. They also want to thank Sebastian Scheiding and Marian Wiemuth for performing some basic investigations and for many fruitful discussions. Parts of the research were supported by the German Aerospace Center DLR within the project *ultraLEICHT* under grant number 50EE1408.

REFERENCES

-
- [1] Á.R. Machado, J. Wallbank, Proc. Inst. Mech. Eng. **204**, 53 (1990). doi:10.1243/PIME_PROC_1990_204_047_02
- [2] P.R. Yoder, *Opto-Mechanical Systems Design*, 3rd edn. (CRC Press, 2006)
- [3] R. Steinkopf, A. Gebhardt, S. Scheiding, et al., Proc. SPIE **7102**, 71020C (2008). doi:10.1117/12.797702
- [4] S. Scheiding, C. Damm, W. Holota, et al., Proc. SPIE **7739**, 773908 (2010). doi:10.1117/12.856244
- [5] S. Risse, A. Gebhardt, C. Damm, et al., Proc. SPIE **7010**, 701016 (2008). doi:10.1117/12.789824
- [6] J. Kinast, E. Hilpert, N. Lange, et al., Proc. SPIE **9151**, 915136 (2014). doi:10.1117/12.2056271
- [7] A. Ahmad (ed.), *Handbook of Optomechanical Engineering* (CRC Press, 1996)
- [8] D. Buchbinder, H. Schleifenbaum, S. Heidrich, et al., Physics Procedia **12**, 271 (2011). doi:10.1016/j.phpro.2011.03.035
- [9] E. Louvis, P. Fox, C.J. Sutcliffe, J. Mater. Process. Tech. **211**, 275 (2011). doi:10.1016/j.jmatprotec.2010.09.019
- [10] K.G. Prashanth, S. Scudino, H.J. Klauss, et al., Mat. Sci. Eng. A-Struct. **590**, 153 (2014). doi:10.1016/j.msea.2013.10.023
- [11] P. Vora, K. Mumtaz, I. Todd, et al., Additive Manufacturing **7**, 12 (2015). doi:10.1016/j.addma.2015.06.003
- [12] E. Brandl, U. Heckenberger, V. Holzinger, et al., Mater. Design **34**, 159 (2012). doi:10.1016/j.matdes.2011.07.067
- [13] (2016). URL <http://www.ansys.com>. Electronic address
- [14] (2016). URL http://www.esa.int/Our_Activities/Space_Engineering_Technology/Mirror_mirror_testing_3D_printing_for_space. Electronic address
- [15] M. Sweeney, M. Acreman, T. Vettese, et al., Proc. SPIE **9574**, 957406 (2015). doi:10.1117/12.2189202
- [16] H. Herzog, J. Segal, J. Smith, et al., Proc. SPIE **9573**, 957308 (2015). doi:10.1117/12.2188197
- [17] J. Mici, B. Rothenberg, E. Brisson, et al., Proc. SPIE **9573**, 957306 (2015). doi:10.1117/12.2188533
- [18] J. Kranz, D. Herzog, C. Emmelmann. Laser additive manufacturing of lightweight structures in TiAl6V4: a design for manufacturing approach. Oral presentation, ESA Workshop on additive manufacturing for space application (2014)
- [19] P. Rochus, J.Y. Plessier, A. Corbelli, et al., 65th International Astronautical Congress (2014)
- [20] R. Dehoff, C. Duty, W. Peter, et al., Adv. Mater. Process. **171**, 19 (2013)
- [21] J.P. Kruth, P. Mercelis, J. Van Vaerenbergh, et al., Proc. of VR@P pp. 521 – 527 (2007)
- [22] X. Su, Y. Yang, D. Xiao, et al., Int. J. Adv. Manuf. Technol. **64**, 1231 (2012)
- [23] M. Wiemuth, Experimentelle Untersuchungen zur Leichtbauoptimierung von hohlstrukturierten Metallspiegeln durch Rapid Prototyping. Master's thesis, HAWK Göttingen (2013). Confidential
- [24] D. Buchbinder, G. Schilling, W. Meiners, et al., RTejournal - Forum für Rapid Technologie **8** (2011)
- [25] B. Vrancken, V. Cain, R. Knutsen, et al., Scripta Mater. **87**, 29 (2014). doi:10.1016/j.scriptamat.2014.05.016
- [26] P. Mercelis, J.P. Kruth, Rapid Prototyping J. **12**, 254 (2006). doi:10.1108/13552540610707013
- [27] Q. Bo, S. Yu-sheng, W. Qing-song, et al., Int. J. Adv. Manuf. Technol. **63**, 631 (2012). doi:10.1007/s00170-012-3922-9
- [28] N. Kanani, *Chemische Vernicklung: Nickel-Phosphor-Schichten. Herstellung, Eigenschaften, Anwendungen. Ein Handbuch für Theorie und Praxis* (Eugen G. Leuze Verlag, 2007)
- [29] G.O. Mallory, J.B. Hajdu (eds.), *Electroless Plating: Fundamentals and Applications* (American Electroplaters and Surface Finishers Society, 1990)
- [30] J.S. Taylor, C.K. Syn, T.T. Saito, et al., Opt. Eng. **25**, 1013 (1986). doi:10.1117/12.7973947
- [31] J.W. Dini, Plat. Surf. Finish. **79**, 121 (1992)
- [32] F.C. Walsh, C. Ponce de León, C. Kerr, et al., Surf. Coat. Tech. **202**, 5092 (2008). doi:10.1016/j.surfcoat.2008.05.008
- [33] M. Beier, S. Scheiding, A. Gebhardt, et al., Proc. SPIE **8884**, 88840S (2013). doi:10.1117/12.2035986
- [34] M. Beier, W. Fuhlrott, J. Hartung, et al., Proc. SPIE **9912**, 99120Y (2016). doi:10.1117/12.2230013
- [35] C.W. Marschall, R.E. Maringer, *Dimensional Instability: An Introduction* (Pergamon Press, 1977)